Electronic structure of cobalt / iron carbide from ab-initio calculations

A. Aseema Banu [1], Smagul Zh. Karazhanov [2] and Sujin P. Jose [1]

[1] School of Physics, Madurai Kamaraj University, Madurai-625021, India
[2] Department for Solar Energy, Institute of Energy Technology, 2007 Kjeller, Norway

[*]sujamystica@yahoo.com (Sujin P Jose)

Abstract

This work presents theoretical study of structural and electronic properties of bulk cobalt and iron carbide by the first-principles calculations. Structural optimization has been performed and the ground state properties such as the equilibrium lattice constants, cohesive energy (E_{coh}**)** and bulk modulus (B_0) of Co_2C/η-Fe_2C have been calculated. Band structure, density of states (DOS) and 3D isosurface valence charge density difference for Co_2C and η-Fe_2C has been reported. The experimental and simulated powder X-ray diffraction data were compared and the Miller indices which define the crystallographic planes in the crystal lattices were identified. Mechanical stability of these compounds was discussed in terms of their equilibrium E_{coh} and B_0 values. Our computed values were also compared with the available experimental and theoretical data.

Keywords: First-principle calculations, LDA, GGA, Co_2C, η-Fe_2C, Electronic property, Magnetic property.

1. Introduction

The physicochemical properties of transition metal carbides (TMCs) are highly interesting and focused for both academic research and industrial applications due to their high melting point, hardness, thermal and electrical conductivity as well as superconductivity [1-4]. In the

periodic table, group IIIA carbides are important as precipitates in metallic alloys (iron, cobalt, nickel). The transition metal carbides provide an interesting and important set of diatomic molecules for experimental as well as theoretical study and represent a very active field of research. The η-carbide of iron (or) η-Fe_2C, is orthorhombic and isomorphous with Co_2C and Co_2N. Recent works predicted that orthorhombic Fe_2C is thermodynamically more stable than hexagonal Fe_2C based on computed cohesive energies. Several iron group carbides have also been recently investigated in the gas phase by various research groups and high level spectroscopic results in CoC molecules are explored [5]. TMCs behave like noble metals for electrochemical reaction such as oxidation of hydrogen, carbon monoxide, alcohols and reduction of oxygen [6]. Adrian Oila et al have predicted hardness and elastic properties of η-Fe_2C [7]. Two modifications of the iron carbide have been reported, the so-called eta carbide η-Fe_2C and epsilon carbide ε-$Fe_{2.4}C$ are the two transition metal compounds which occur in the microstructure of quenched steels during the initial stages of tempering [8]. The iron/carbon system is characterized by a solid solution (austenite or ferrite), the well-known θ-Fe_3C (cementite) and other metastable crystalline iron-carbide phases are χ-Fe_5C_2 (Hägg carbide) and η-Fe_2C and the transition metal carbides are in the metastable state from the thermodynamical point of view [9, 10]. TMCs exhibit excellent catalytic properties and have been the focus of many research fields of catalysis and surface science [11]. The catalytic performance ranges from hydrogenation, dehydrogenation, hydrogenolysis and Fischer-Tropsch synthesis (FTS) etc, that approaches or surpassing those of precious Pt-group metals. Formation of carbide, especially Co_2C, is often referred to as a sign of deactivation. Active components on cobalt catalysts are usually considered to remain in metallic states during FTS [12]. In addition, Cheng et al reported [13] the results of catalytic properties of Fe and Co carbides (χ-Fe_5C_2 and Co_2C) by first-

principles calculations within GGA suggested that Fe carbide is more active and Co carbide is less active in high methane selectivity of the process of FTS. There are several theoretical and experimental studies on bulk Co_2C, Zhao et al has studied [11] structural and electronic properties of bulk Co_2C within GGA. Stability of low index Co_2C surface and also the density of states (DOSs) reveal that the Co_2C is paramagnetic, and is metallic. The difference of charge density analysis indicates that the bond of Co_2C is of the mixtures of metallic, covalent and ionic properties and also predicted that the material Co_2C is non-magnetic. Fang et al investigated [14] that the comparison of electronic structure calculations for Fe_2X (X = C, N) phase and also analyzed the chemical bonding and charge transfer of N and C ions. In this work, a first principle study was carried out for the comparison of the structural and electronic properties Co_2C and η-Fe_2C using different PP, specifically PAW versus US, for both the LDA and GGA which has not been addressed so far. The achieved insights are important in computational materials research and the parameters can be fitted experimentally.

2. Computational details

2.1 Geometry optimization

Vienna Ab-initio Simulation Package has been used in the computations [15]. Ultra-soft pseudopotentials (US-PP) [16] and projected augmented wave pseudopotentials (PAW-PP) [17, 18] have been used. Exchange and correlation were approximated using either the LDA adapted by Ceperly and Alder [19] or the GGA of Perdew and Wang [20]. The crystal structure of Co_2C and η-Fe_2C has an orthorhombic bulk structure belongs to the space group *Pmnn* (No.58) [21] and *Pnnm* (No.58) [22] respectively. The valence electronic configurations taken as Co ($4s^1\ 3d^8$), Fe ($4s^1\ 3d^7$) and C ($2s^2\ 2p^2$) atoms and the atomic radii of Co, Fe and C atoms are 1.25, 1.26 and 0.77 Å respectively. The maximum value l_m for the wave function expansion inside the atomic

sphere is limited to 10. All calculations were performed using the plane-wave cutoff energy is 300 eV for US-PP and 400 eV for PAW-PP, and assured a very high level convergence with respect to the total energy difference within 1.0×10^{-4} (eV/atom), likewise 680 plane waves for US-PP and 1059 plane waves for PAW-PP were used for both Co_2C and η-Fe_2C. Brillouin zone integrations are performed on the Monkhorst-Pack K-point mesh with a grid size of 6 x 4 x 4 / 4 x 4 x 6 (12 irreducible K points) for US-PP and 8 x 6 x 6 / 6 x 6 x 8 (36 irreducible K points) for PAW-PP were used for all calculations. Figure 1(a) presents schematic design of the lattice of Co_2C with one C atom is in the center of the unit cell and eight C atoms are on the corners of the unit cell, with each C atom shared by the neighboring eight unit cells; there are two Co atoms in the unit cell and four Co atoms on the planes shared by the neighboring two unit cells. As a result, each unit cell contains 4 Co atoms and 2 C atoms for Co_2C and similarly 4 Fe atoms and 2 C atoms for η-Fe_2C as shown in figure 1(b).

3. Results and discussions

3.1. Structural properties

The combination of metals with light covalent-bond forming atoms like B, C and N often leads to materials which not only have a high melting point, but also have a very low compressibility and high hardness compared with the pure metal [23]. The ground state properties of Co_2C and η-Fe_2C are investigated from their total energy, which is calculated as a function of volume and these values are fitted to the Birch-Murnaghan equation of state (EOS) [24] as shown in figure 2 and figure 3 for Co_2C and η-Fe_2C respectively,

$$\boldsymbol{E}\,(\mathbf{V}) = \mathbf{E_0} + \mathbf{9V_0B_0/16}\{[(\mathbf{V_0}/\mathbf{V})^{\mathbf{2/3}} - \mathbf{1}]^{\mathbf{3}}\boldsymbol{B'_0} + [(\mathbf{V_0}/\mathbf{V})^{\mathbf{2/3}} - \mathbf{1}]^{\mathbf{2}}[\mathbf{6} - \mathbf{4}(\mathbf{V_0}/\mathbf{V})^{\mathbf{2/3}}]\} \quad \textbf{(1)}$$

to determine the equilibrium lattice constants, cell volume and bulk modulus. As listed in table 1, it can be found that the GGA values of the lattice constants match fairly well with the

experimental data (the error less than 1 %). For the Co_2C, the calculated lattice parameters of a_0, b_0 and c_0 within LDA are lesser than experimental values by approximately 2.8 %, while the GGA values are smaller by approximately 0.7 %. Similarly, in the case of η-Fe_2C, the calculated lattice parameters of a_0, b_0 and c_0 within LDA are smaller than experimental values by approximately 2.8 %, but, in GGA, there is no deviation from the experimental values. Hence, the error of LDA is bigger than that of GGA for both Co_2C and η-Fe_2C. For comparing the stability of these materials, cohesive energy defined in the equation is used [27, 28]

$$\mathbf{E_{coh} = (\sum_A^{gs} E + \sum_B^{gs} E - E\,(Bulk))/\,N_A + N_B} \qquad \mathbf{(2)}$$

Where E (Bulk) is the bulk energy of cobalt/ iron carbide, $\sum_A^{gs} E$ is the ground states energies of Co / Fe atom in the unit cell, $\sum_B^{gs} E$ is the ground state energy of C atom in the unit cell and N_A is the number of Co / Fe atoms in the bulk, N_B is the number of C atoms in the bulk. It is found that the Co_2C is more stable than the η-Fe_2C by 0.53 eV and 0.13 eV based on the computed cohesive energy for GGA-US and PAW respectively. The calculated bulk modulus values indicate that the Co_2C having more strength and hardness than η-Fe_2C by 43 Gpa and 45 Gpa for GGA-US and PAW correspondingly. Figure 1(a) and (b) shows that, in bulk Co_2C/η-Fe_2C, each C atom binds with six Co/Fe atoms and each Co/Fe atoms binds with three C atoms. The optimized Fe-C distances are 0.1904 and 0.1945 nm, close to the experimental values (0.1904 and 0.1945 nm) [24] and similarly, Co-C distances are 0.1918 and 0.1911 nm, close to the theoretical value (0.193 nm) [13]. To the best of our knowledge, the experimental and theoretical values of cohesive energy and bulk modulus of Co_2C have not been reported so far. Hence the present work provides useful insights for the experimental researchers.

3.2. Density of states

To obtain further understanding about the interaction between cobalt / iron and carbon in bulk at equilibrium state, the total density of states (TDOS) and partial density of states (PDOS) with respect to the different atoms were computed and plotted. This yields the contribution of the *s*, *p* and *d*-states to the TDOS for spin polarized calculation (up and down) by the standard tetrahedron method. The TDOS (Figure **4** (a) and **4** (b)) and PDOS (Figure **6** (a) and **6** (b)) shows that projected onto Co and C contributions for Co_2C using functional GGA (US and PAW) at normal pressure and it consists of three regions: Two valence regions, the lower lying valence band (VB2) and the upper lying valence band (VB1) below E_F and one conduction band (CB) above E_F, the last two regions (VB1 and CB) are highly overlapped to each other. The Fermi energy level (E_F) is set to zero. The lower VB2 is dominated by C 2*s* states mainly. The upper VB1 is strongly originated from C 2*p* states with the little contribution of Co 4*p* and 3*d* states and constitute the strong interaction between C 2*p* states and Co 3*d* states; the CB is mostly formed by Co 3*d* states. It is observed that the Co 3*d* electrons are mainly contributed to the DOS at the E_F and in the conduction properties. It is seen from the histograms, the spin-up and spin-down densities of states of all the above bands are almost symmetric, which indicate that the non-magnetic properties of Co_2C. No energy gap near the E_F can be seen, due to density of states (spin up and down) at the Fermi energy $N\uparrow(E_F)$ = 1.775 states/eV per formula unit and $N\downarrow(E_F)$ = 4.1 states/eV per formula unit, $N\uparrow(E_F)$ = 2.030 states/eV per formula unit and $N\downarrow(E_F)$ = 2.0332 states/eV per formula unit for Co_2C (GGA-US and PAW respectively). These values in turn validate the metallic nature of Co_2C. The calculated TDOS (Figure **5** (a) and **5** (b)) and the PDOS (Figure **7** (a) and **7** (b)) show the estimated contributions from Fe and C for η-Fe_2C using functional GGA (US and PAW). The 2*s* states of C mainly contributed to their lower energy

VB2. The 2*p* states of C mainly contribute to the lower portions of VB1 along with the small contribution of 4*p* and 3*d* states of Fe, which indicate that there are strong covalent features between C 2*p* and Fe 3*d* states. Interestingly, the 3*d* states of Fe, largely contribute to the higher portions of their VB1 (just below the E_F) and the lower portion of their CB (just above the E_F). Hence, the 3*d* states of Fe electrons play an important role in the conducting properties. On comparing, the up and down densities of states were found to be asymmetric, which indicate that the magnetic properties of η-Fe_2C. It is found that, there is no band gap due to density of states (spin up and down) at the Fermi energy $N\uparrow(E_F)$ = 0.6825 states/eV per formula unit and $N\downarrow(E_F)$ = 3.945 states/eV per formula unit, $N\uparrow(E_F)$ = 1.078 states/eV per formula unit and $N\downarrow(E_F)$ = 4.668 states/eV per formula unit for η-Fe_2C (GGA-US and PAW respectively). These values, in turn, authenticate the metallic nature of η-Fe_2C. In the case of GGA-PAW, both cobalt carbide and iron carbide were calculated to be non-magnetic and ferromagnetic respectively. The large differences for the DOSs at the E_F for the spin-up ($N\uparrow[E_F]$) and spin-down ($N\downarrow[E_F]$) electrons indicate the magnetic nature of η-Fe_2C. Therefore, the degree of spin-polarization $\mathbf{P = \{[N\uparrow(E_F) - N\downarrow(E_F)]/[N\uparrow(E_F) + N\downarrow(E_F)]\}}$ = 62 % for η-Fe_2C and P = 7.8 x 10^{-6} % for Co_2C. These results indicate that η-Fe_2C can be acted as potential candidate for applications in spintronics and magnetic recording media [**14**]. The previous studies have shown that Co_2C, as well as, η-Fe_2C are metallic in nature. But the magnetic moments were quite different for the two carbides: η-Fe_2C [**29**] has magnetic characteristic while the Co_2C [**11**] has non-magnetic characteristic. Table **1** listed out the calculated local magnetic moments for individual ions as per unit cell and these agreed well with the available data. The net magnetization of Co_2C is almost vanished, about 0.73 / 0.002 μ_B per unit cell (Co_2C) and similarly, 6.53/ 6.06 μ_B per unit cell (η-Fe_2C) for GGA-US and PAW respectively.

3.3 Electronic Band Structure

Transition metal carbides, nitrides and borides are a large and complex group of industrially relevant compounds with outstanding physical properties. The most macroscopical properties of a material, such as hardness, elasticity, metallic property and superconductivity are closely connected to its electronic structure and chemical bonding character [30]. Thus, it is vital to investigate the electronic structure for Co_2C and η-Fe_2C along selected high symmetry directions X-G-Z-U-G-Y-T-G-R are located in the first Brillouin zone figure **8** and figure **9** respectively, where the Fermi energy level is set to zero. From the figure **8,** it is observed that below the Fermi level, an actively low-lying band, ranging from -13.94 eV to -11.39 eV, is clearly apart from the higher one. It is created from the C 2*s* states even if it does not contribute to the bonding between the Co and C atoms. As the energy scale increases, the C 2*p* and Co 3*d* orbitals form a suitable hybrid orbital below the Fermi level, extending up to 1.0 eV, above the Fermi energy, which contributes to the covalent bond between the C and Co atoms. The energy bands above 1.0 eV are mostly derived from the delocalized Co 3*d* and 4*p* orbitals. From figure **9**, η-Fe_2C is characterized by an energetically low lying doubly degenerate band at X, U and T points which is derived from the 2*s* states of carbon atom. The remaining bands are due to C 2*p* and Fe 3*d* states. The conduction bands above the Fermi level are due to delocalized Fe 3*d* states with the little contribution of Fe 4*p* states. The valence and conduction bands are highly overlapped which authenticates the metallic nature of the cobalt and iron carbide.

3.4 Charge density difference

To demonstrate the chemical bonding nature, the computed and plotted 3D isosurface valence charge density difference are shown in figure **10** for Co_2C (pink spheres represents - Co atoms ;

brown spheres - C atoms) and figure 11 for η-Fe_2C (grey spheres represents - Fe atoms ; brown spheres - C atoms).

$$\Delta\rho = \rho_{AB-} \rho_{A-} \rho_{B} \quad (3)$$

Where ρ_{AB} and $\rho_{A,}$ ρ_{B} are the valence electron densities for the bulk system and the corresponding free atoms separately [31]. The charge density around the Co/Fe and C ions is high while there is hardly a valence charge in the tetrahedron-hole interstitial region. Some fraction of electrons are transferred from carbon to cobalt / iron and also cobalt / iron to carbon, which clearly shows the existence of a strong direct bonding between Co/Fe and C atoms that is, a covalent bonding between carbon and cobalt / iron atom. Furthermore, there is depletion of electrons around Co/Fe atoms, it's denoted by blue lobe and charge accumulation with the distance nearer to carbon, due to C (2.55) has more electronegative than Co (1.88) and Fe (1.83), it's represents yellow lobe and reveals an ionic contribution between positively charged Co/Fe and negative charged C to the bonding. The isovalue is set at 0.016 e / $Bohr^3$ for both systems. Therefore, our results demonstrate that the bonds of Co_2C and η-Fe_2C are the unusual mixtures of metallic, covalent and ionic nature.

3.5 X-ray diffraction studies

The powder X-ray Diffraction (PXRD) patterns of Co_2C and η-Fe_2C using VESTA software, theoretically analyzed and shown in figure 12 and figure 13 respectively. PXRD patterns were plotted over the 2θ ranging from 0^o to 120^o with wavelength (λ = 0.15405 nm) for both cobalt carbide as well as iron carbide. The experimental one was compared with the simulated one and found to be agreeing with each other. The sharp and well defined Bragg's peaks at specific 2θ angle testimonies the crystalline nature of the sample. The Miller indices which define the lattice place of Co_2C and η-Fe_2C were predicted and are mentioned in table 2 and table 3 respectively.

In figure 12, the (002) peak corresponds to the orthorhombic structure of Co_2C (d_{002}= 2.17Å; 2θ = 41.58°). The obtained XRD pattern is close to the standard reported in the JCPDS crystallographic database [32]. As seen in this figure, all the peaks in the XRD could be indexed only for Co_2C and there is no extra XRD peak is found. In figure 13, the (020) peak corresponds to the orthorhombic structure of η-Fe_2C (d_{020}= 2.16 Å; 2θ = 41.8°). The simulated XRD pattern is close to the standard reported in the JCPDS crystallographic database [33]. It is observed that, all the peaks in the XRD could be indexed only for η-Fe_2C and there is no extra XRD peak is found. The highest peaks are appeared around 42^o is indexed for cobalt carbide and iron carbide structures with an orientation at zone axes of [002] and [020] planes respectively. The above results confirm the orthorhombic structure of cobalt carbide and iron carbide.

4. Conclusions

In summary, the ab initio calculations were performed to study structural, electronic and magnetic properties of Co_2C and η-Fe_2C. The theoretically calculated and experimentally established lattice parameters, bulk modulus and cohesive energy agree very well with each other. Co_2C and η-Fe_2C were established to be stable in the orthorhombic structure at ambient pressure. The density of states and band structure reveal that the Co_2C is non-magnetic and exhibit strong metallic behavior, but η-Fe_2C is magnetic and demonstrates strong metallic-nature. The difference of charge density indicates that the bonds of Co_2C, as well as, η-Fe_2C are of the mixtures of metallic, covalent and ionic properties. These findings will provide beneficial insights to the research community who are interested to work on the TMCs.

References

[1] Goldschmidt H Interstitial Alloys 1967 Butterworths London.

[2] Toth LE Transition Metal Carbides and Nitrides 1971 Academic Press: New York.

[3] Schwarz K 1987 CRC Crit. Rev Solid State Mater. Sci. 13 (3) 211.

[4] Gubanov V A Ivanovskii A L and Zhukov V P (1994) Cambridge University Press: Cambridge.

[5] Brewster M A and Ziurys L M 2001 The Astrophysical Journal 559 (2) L163-L166.

[6] Dong Jin Ham and Jae Sung Lee 2009 Energies 2 (4) 873-899.

[7] Adrian Oila Chi Lung and Steve Bull 2014 Journal of Materials Science 49 (5) 2383-2390**.**

[8] Nakamura Y and Nagakura S 1986 Transactions of the Japan.Institute of Metals 27 (11) 842.

[9] Faraoun H I Zhang Y D Esling C and Aourag H 2006 J. Appl. Phys 99 (9) 093508.

[10] Fang C M van Huis M A and Zandbergen H W 2010 J. scriptamat 63 (4) 418-421.

[11] Yong-Hui Zhao Hai-Yan Su Keju Sun Jinxun Liu and Wei-Xue Li 2012 Surface Science 606 598-604.

[12**]** Xiong J Ding Y Wang T and Yan L 2005 Catal. Lett 102 (3-4) 265.

[13] Jun Cheng and Hu P 2010 J. Phys. Chem. C 114 (2) 1085-1093.

[14] Fang C M van Huis M A Jansen J and Zandbergen H W 2011 Phys. Rev. B 84 (9) 094102.

[15] Kresse G and Furthmuller J 1996 Phys. Rev. B 54 (16) 11169.

[16] Vanderbilt D 1990 Phys. Rev. B 41 (11) 7892.

[17] Blochl P E 1994 Phys. Rev. B 50 (24) 17953.

[18] Kresse G and Joubert D 1999 Phys. Rev. B 59 (3) 1758.

[19] Ceperley D M and Alder B J Phys. Rev. Lett 45 (7) (1980) 566.

[20] Perdew J P Chevary J A Vosko S H Jackson K A Pederson M R and Singh D 1992 J Phys. Rev. B 46 (11) 6671.

[21] Clarke J and Jack K H 1951 Chem. Ind London 1004.

[22] Hirotsu Y and Nagakura S 1972 Acta. Met 20 (4) 645-655.

[23] Alexandra Friedrich Björn Winkler Erick A. Juarez-rellano and Lkhamsuren Bayarjargal 2011 Materials 4 (10) 1648-1692.

[24] Murnaghan F D 1944 Proc. Natl. Acad. sci 30 (9) 244-247.

[25] Ande C K and Sluiter M H 2012 Metallurgical and Materials Transactions A 43A 4436.

[26] BAO Li-li HUO Chun-fang DENG Chun-mei and LI Yong-wang 2009 Journal of Fuel Chemistry and Technology 37 (1) 104.

[27] Wun C Chiou Jr and Emily A 2003 Carter Surface Science 530 87-100.

[28] Su J Pei Y Yang Z and wang X 2015 RSC Adv 5 (35) 27229-27234.

[29] Lv Z Q Sun S H Jiang P Wang B Z and Fu W T 2008 J. Commat. Sci 42 (4) 692-697.

[30] Yang Xiao-Yong Lu Yong Zheng Fa-Wei and Zhang Ping 2015 Chin. Phys. B 24 (11) 116301.

[31] Shein I R Medvedeva N I Ivanovskii A L 2006 Physica B 371 (1) 126-132.

[32] Joint Committee on Powder Diffraction Standards - JCPDS. Crystallographic data base. PDF #72-1369.

[33] Joint Committee on Powder Diffraction Standards - JCPDS. Crystallographic database. PDF # 89-5901.

Compound	Method / PP *	a (Å) Err, %	b (Å) Err, %	c (Å) Err, %	V_0(Å^3) Err, %	B_0 (Gpa)	E_{coh} (eV)	M_{TM} (μB)	M_C (μB)
Co_2C Present work	LDA-CA/US	2.815 2.797	4.322 2.789	4.248 2.792	51.7 8.17	489	7.37	0.002	-0.00
	LDA-CA/PAW	2.815 2.797	4.322 2.789	4.248 2.792	51.7 8.17	338	7.50	0.001	-0.00
	GGA-PW91/US	2.876 0.691	4.415 0.697	4.340 0.686	55.1 2.13	277	6.282	0.195	-0.022
	GGA-PW91/PAW	2.876 0.691	4.415 0.697	4.340 0.686	55.1 2.13	269	6.191	0.001	-0.00
Previous work	GGA-PBE/ NC [13]	2.920	4.478	4.410	57.7	---	---	---	---
	GGA-PW91/ PAW [11]	2.877	4.386	4.354	54.9	---	---	---	---
	Expt. [21]	2.896	4.446	4.370	56.3	---	---	---	---
η-Fe_2C Present work	LDA-CA/US	4.609 2.103	4.231 1.168	2.773 1.806	54.1 4.92	309	7.205	1.531	-0.098
	LDA-CA/PAW	4.572 2.889	4.197 1.962	2.750 2.620	52.7 7.38	329	7.388	1.414	-0.075
	GGA-PW91/US	4.708 0.000	4.281 0.000	2.824 0.000	57.4 0.000	234	5.755	1.725	-0.196
	GGA-PW91/PAW	4.708 0.000	4.281 0.000	2.824 0.000	57.4 0.000	224	6.059	1.582	-0.119
Previous work	GGA-US [7]	4.722	4.271	2.835	57.1	223	---	---	---
	GGA-PBE [26]	4.651	4.258	2.805	55.5	---	6.18	1.70	0.22
	GGA-PW91[9]	4.687	4.261	2.830	56.5	243	---	1.66	-0.12
	LDA-CA/ US [29]	4.411	4.264	2.778	52.25	253	---	---	---
	GGA-PBE/ US [29]	4.677	4.293	2.814	56.50	226	---	---	---
	Expt.[22,25]	4.708	4.281	2.824	57.4	---	---	---	---

Table 1. Optimized lattice constants (a, b, and c) (Å) and cell volume V_0 (Å^3), bulk modulus (B_0) (Gpa), cohesive energy E_{coh} (eV) and the local magnetic moments in the atomic spheres (μB/atom). * PP – Pseudopotentials, TM - Co / Fe.

Cobalt carbide Co_2C									
Experimental					Simulated				
h	k	l	2θ	Int	h	k	l	2θ	Int
0	1	1	28.615	46	0	1	1	28.82121	6.34914
1	1	0	37	277	1	1	0	37.27681	39.797
0	2	0	40.544	30	0	2	0	40.842	8.486
0	0	2	41.279	343	0	0	2	41.58281	100
1	1	1	42.571	999	1	1	1	42.88526	73.61275
0	2	1	45.75	505	0	2	1	46.09099	75.60126
0	1	2	46.252	8	0	1	2	46.59695	0.56089
1	2	1	56.194	7	1	2	1	56.62579	0.38986
1	1	2	56.628	211	1	1	2	57.06304	16.67708
0	2	2	59.242	37	0	2	2	59.70097	5.91563
2	0	0	64.256	86	2	0	0	64.7633	28.25289
0	3	1	66.567	1	0	3	1	67.09776	0.02455
0	1	3	67.612	1	0	1	3	68.15341	0.01077
1	2	2	68.284	2	1	2	2	68.83206	0.17077
1	3	0	71.435	101	1	3	0	72.01607	17.55163
1	0	3	72.573	5	1	0	3	73.16698	0.77911
1	3	1	75.152	10	1	3	1	75.77386	0.86198
1	1	3	76.145	94	1	1	3	76.77872	8.32927
0	2	3	78.416	55	0	2	3	79.07583	9.79772
2	2	0	78.798	8	2	2	0	79.46276	0.81753
2	0	2	79.289	52	2	0	2	79.95881	9.25112
2	2	1	82.406	92	2	2	1	83.11517	8.3884
1	3	2	85.992	69	1	3	2	86.74686	6.51418
0	4	0	87.729	10	0	4	0	88.50651	3.67211
0	0	4	89.654	21	0	0	4	90.459	8.14127

Table 2. Comparison of experimental and simulated PXRD data for Co_2C.

Iron carbide (η-Fe_2C)									
Experimental					Simulated				
h	k	l	2θ	Int	h	k	l	2θ	Int
1	1	0	28.028	27	1	1	0	28.02749	4.14515
1	0	1	37.042	180	1	0	1	37.04189	29.41248
0	1	1	37.985	10	0	1	1	37.9844	1.36171
2	0	0	38.235	82	2	0	0	38.23506	26.8224
0	2	0	41.806	300	0	2	0	41.80563	100
1	1	1	42.731	999	1	1	1	42.73097	83.66678
2	1	0	43.794	453	2	1	0	43.79414	77.1283
1	2	0	46.229	1	1	2	0	46.22882	0
2	1	1	54.995	3	2	1	1	54.99439	0.29178
1	2	1	57.071	149	1	2	1	57.07056	13.43506
2	2	0	57.935	70	2	2	0	57.93447	12.68963
3	1	0	63.02	1	3	1	0	63.02004	0.16346
0	0	2	65.965	70	0	0	2	65.96449	26.90861
3	0	1	68.337	121	3	0	1	68.33668	23.50038
1	1	2	73.141	1	1	1	2	73.14055	0.08991
0	3	1	73.8	1	0	3	1	73.79951	0.08693
1	3	1	76.976	96	1	3	1	76.97543	9.80301
2	3	0	77.723	47	2	3	0	77.72219	9.4684
2	0	2	78.885	11	2	0	2	78.88487	2.18528
0	2	2	81.216	45	0	2	2	81.21581	9.30002
4	0	0	81.842	5	4	0	0	81.84142	1.92293
2	1	2	82.581	73	2	1	2	82.58047	7.67576
3	2	1	83.422	81	3	2	1	83.42161	8.50013
4	1	0	85.512	32	4	1	0	85.5111	6.8561
2	3	1	86.304	1	2	3	1	86.30314	0.05179

Table 3. Comparison of experimental and simulated PXRD data for η-Fe_2C.

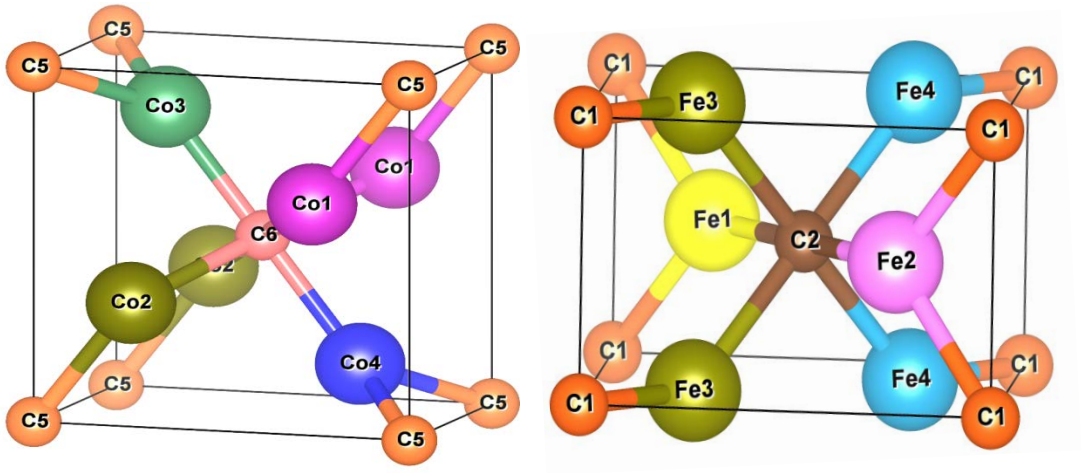

(a) **(b)**

Fig 1. The crystal structure of orthorhombic (a) Co_2C and (b) η-Fe_2C.

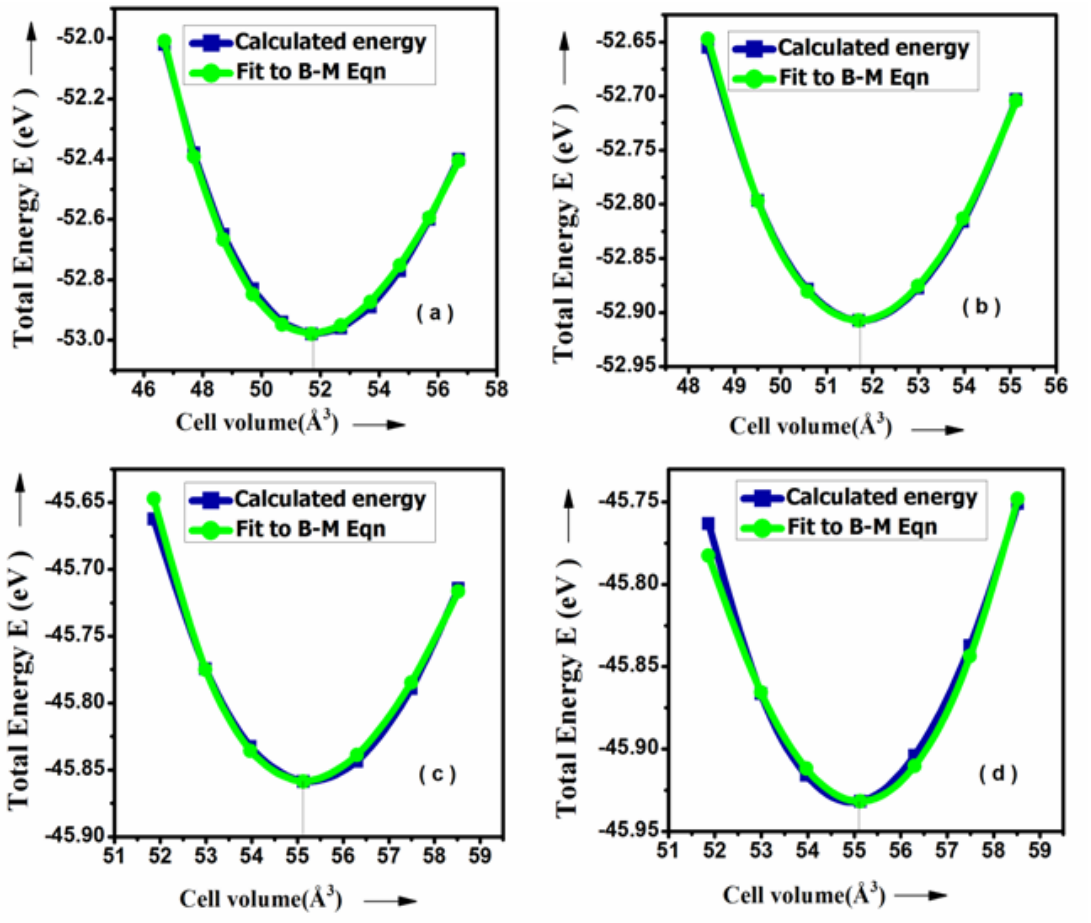

Fig 2. Calculated total energy (eV) as a function of cell volume (Å^3) of Co_2C. (a) LDA-US, (b) LDA-PAW, (c) GGA-US and (d) GGA-PAW.

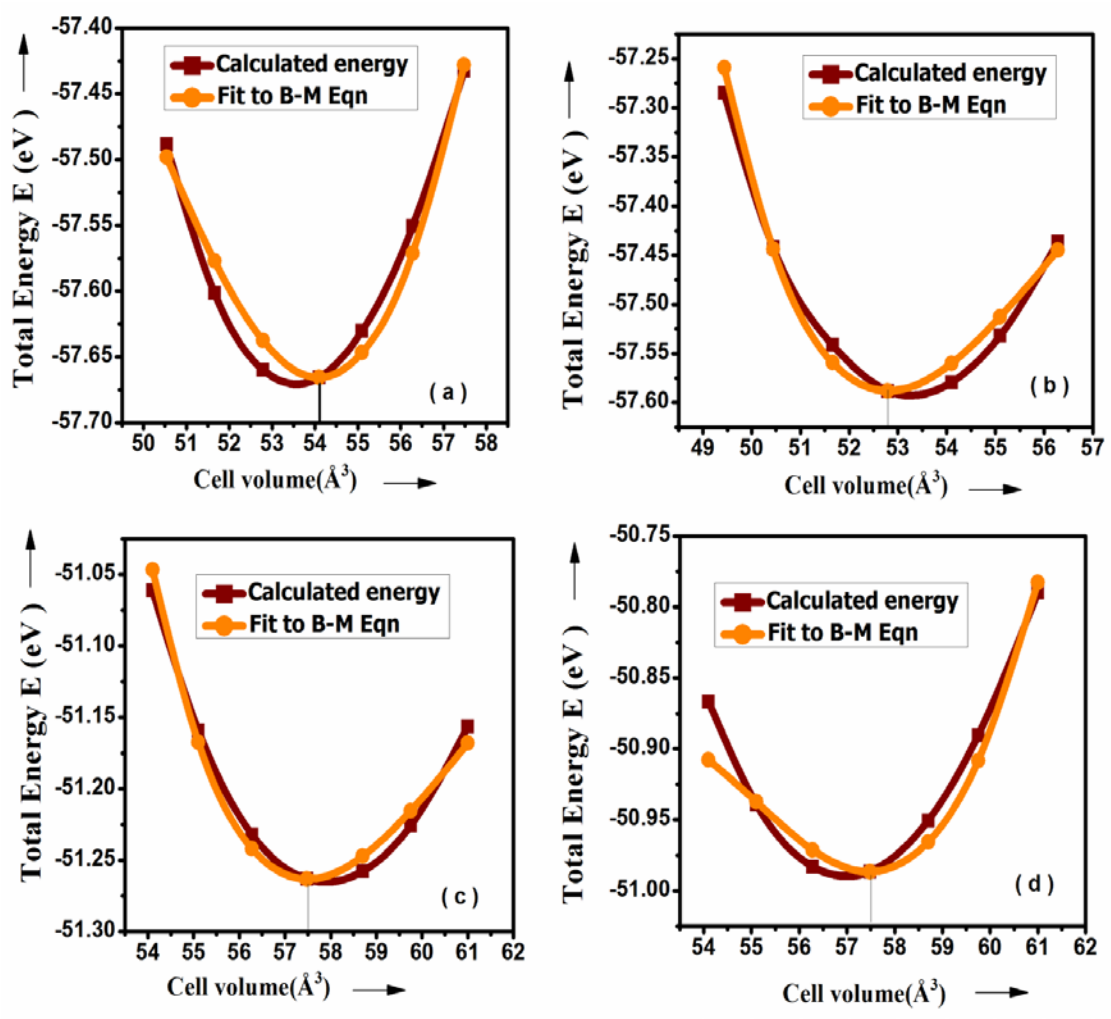

Fig 3. Calculated total energy (eV) as a function of cell volume (Å^3) of η-Fe_2C. (a) LDA-US, (b) LDA-PAW, (c) GGA-US and (d) GGA-PAW.

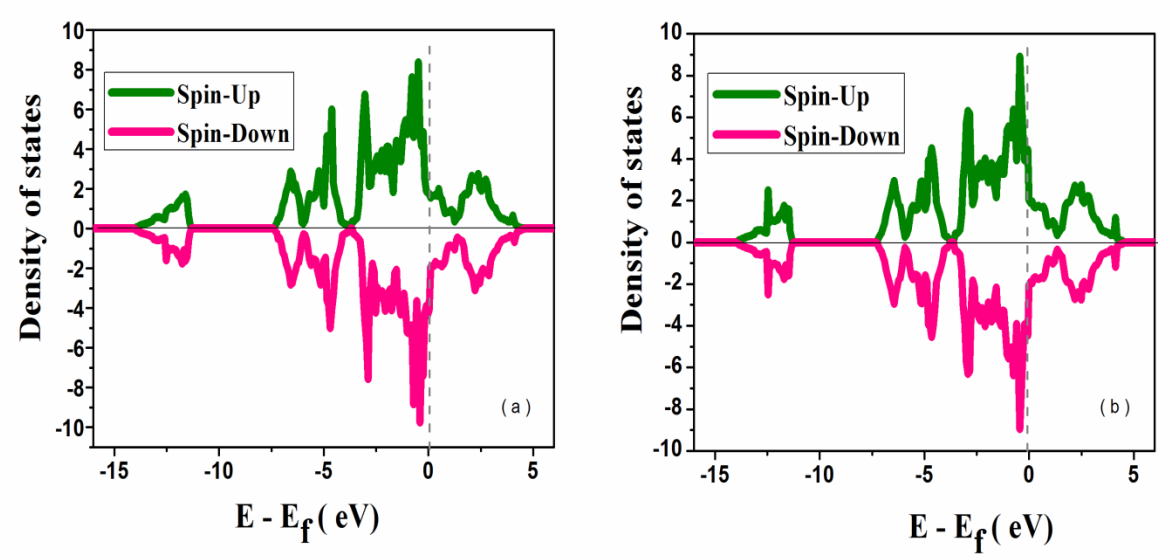

Fig 4. Calculated total density of states (TDOS) of Co_2C. (a) GGA-US and (b) GGA-PAW.

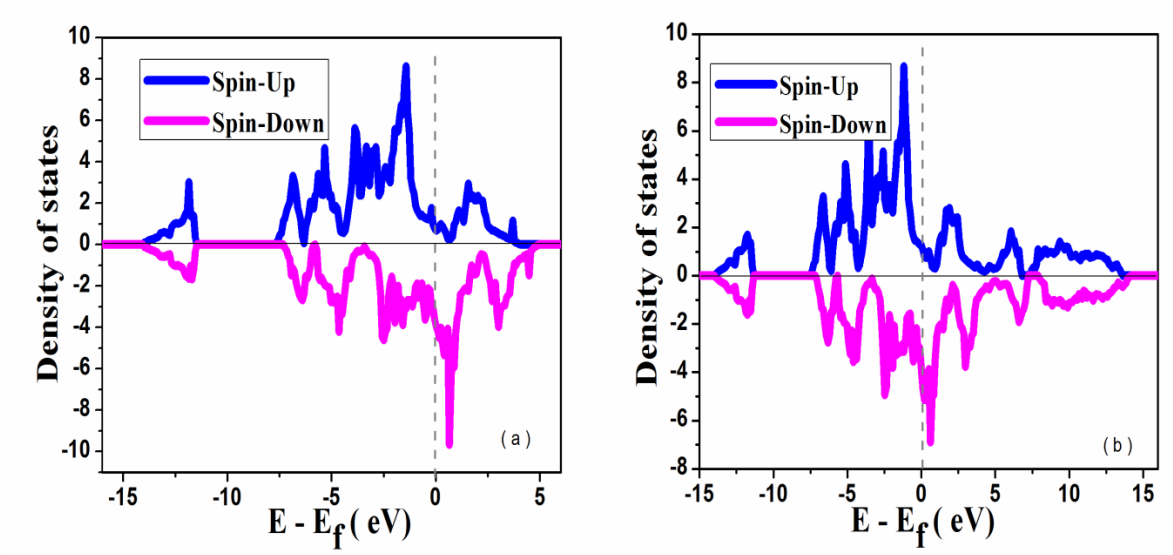

Fig 5. Calculated total density of states (TDOS) of η-Fe_2C. (a) GGA-US and (b) GGA-PAW.

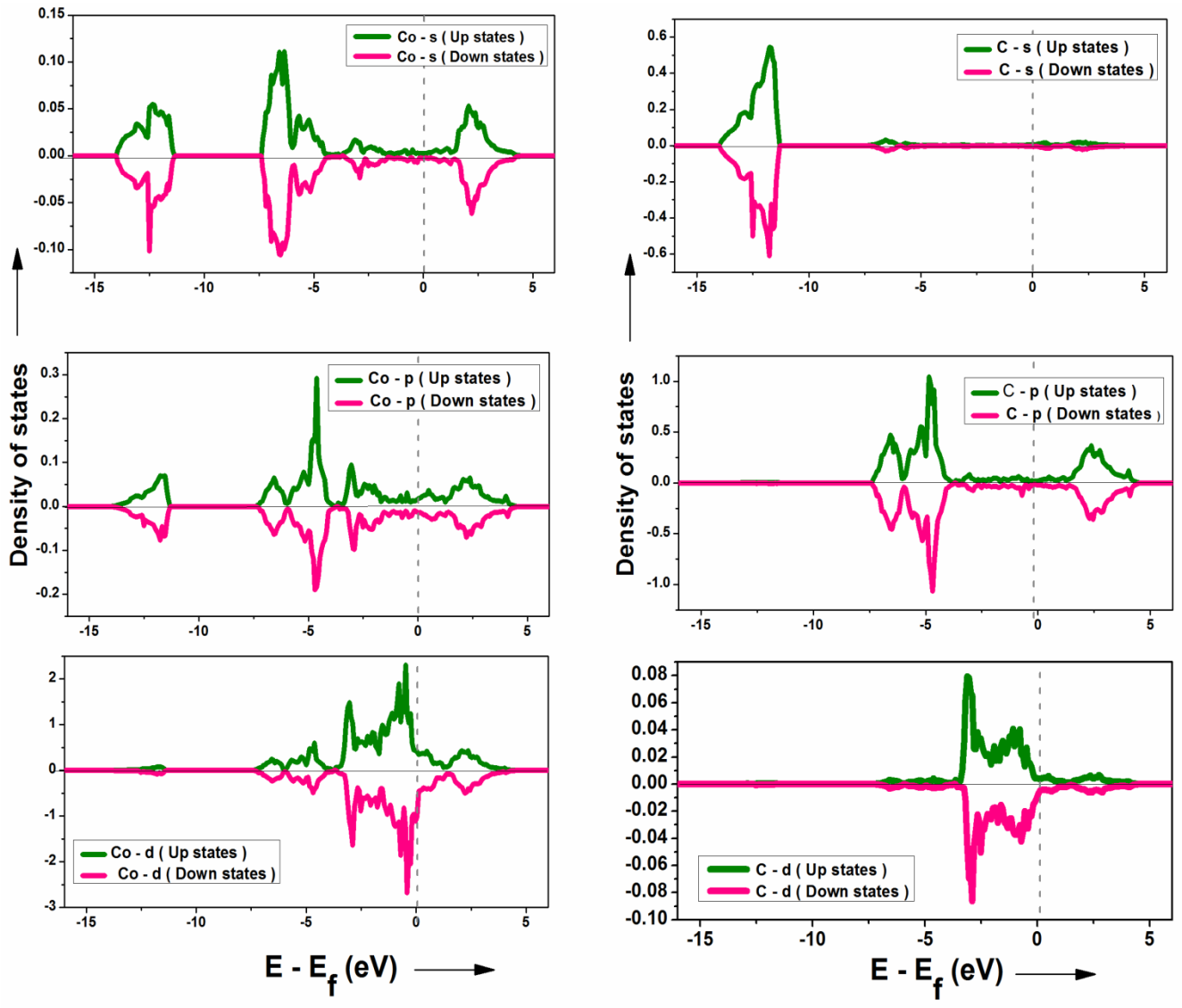
Co - s (Up states)
Co - s (Down states)
C - s (Up states)
C - s (Down states)
Co - p (Up states)
Co - p (Down states)
C - p (Up states)
C - p (Down states)
Co - d (Up states)
Co - d (Down states)
C - d (Up states)
C - d (Down states)
Density of states
Density of states
E - E_f (eV)
E - E_f (eV)

(a)

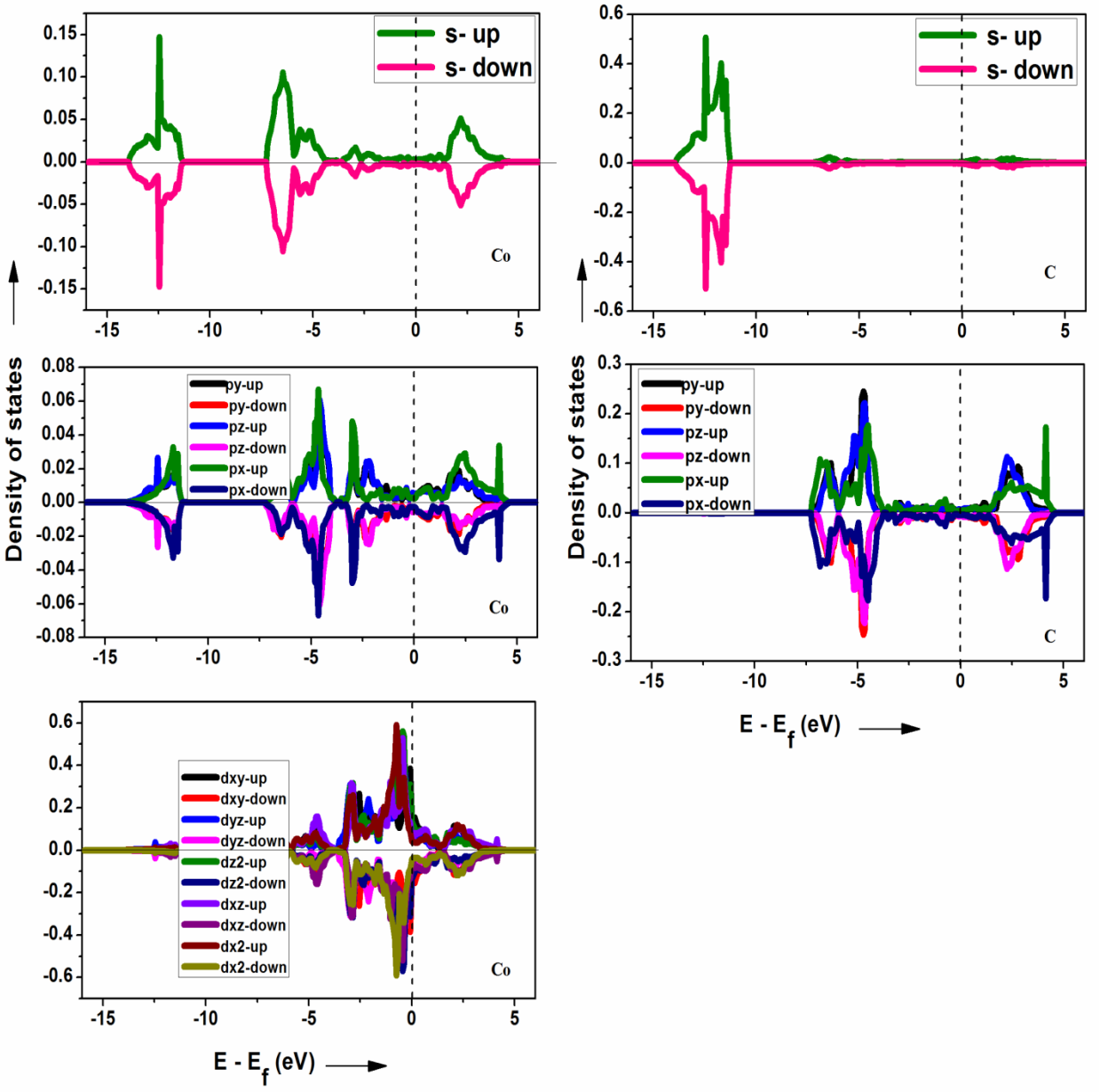

(b)

Fig 6. Partial densities of states (PDOS) of Co_2C for spin-up and down states**.**

(a) GGA-US and (b) GGA-PAW.

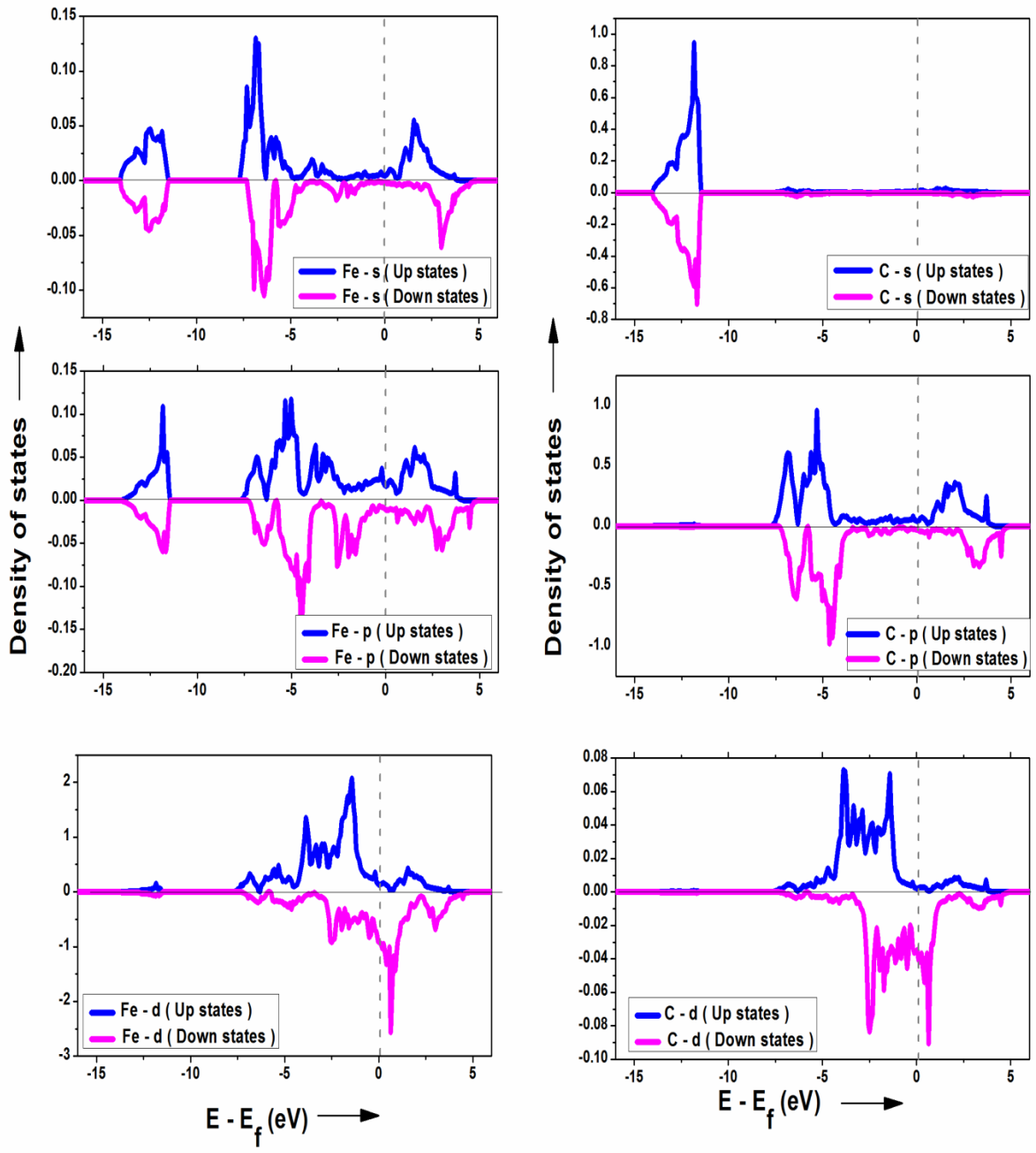
Density of states
Fe - s (Up states)
Fe - s (Down states)
C - s (Up states)
C - s (Down states)
Fe - p (Up states)
Fe - p (Down states)
C - p (Up states)
C - p (Down states)
Fe - d (Up states)
Fe - d (Down states)
C - d (Up states)
C - d (Down states)
E - E_f (eV)

(a)

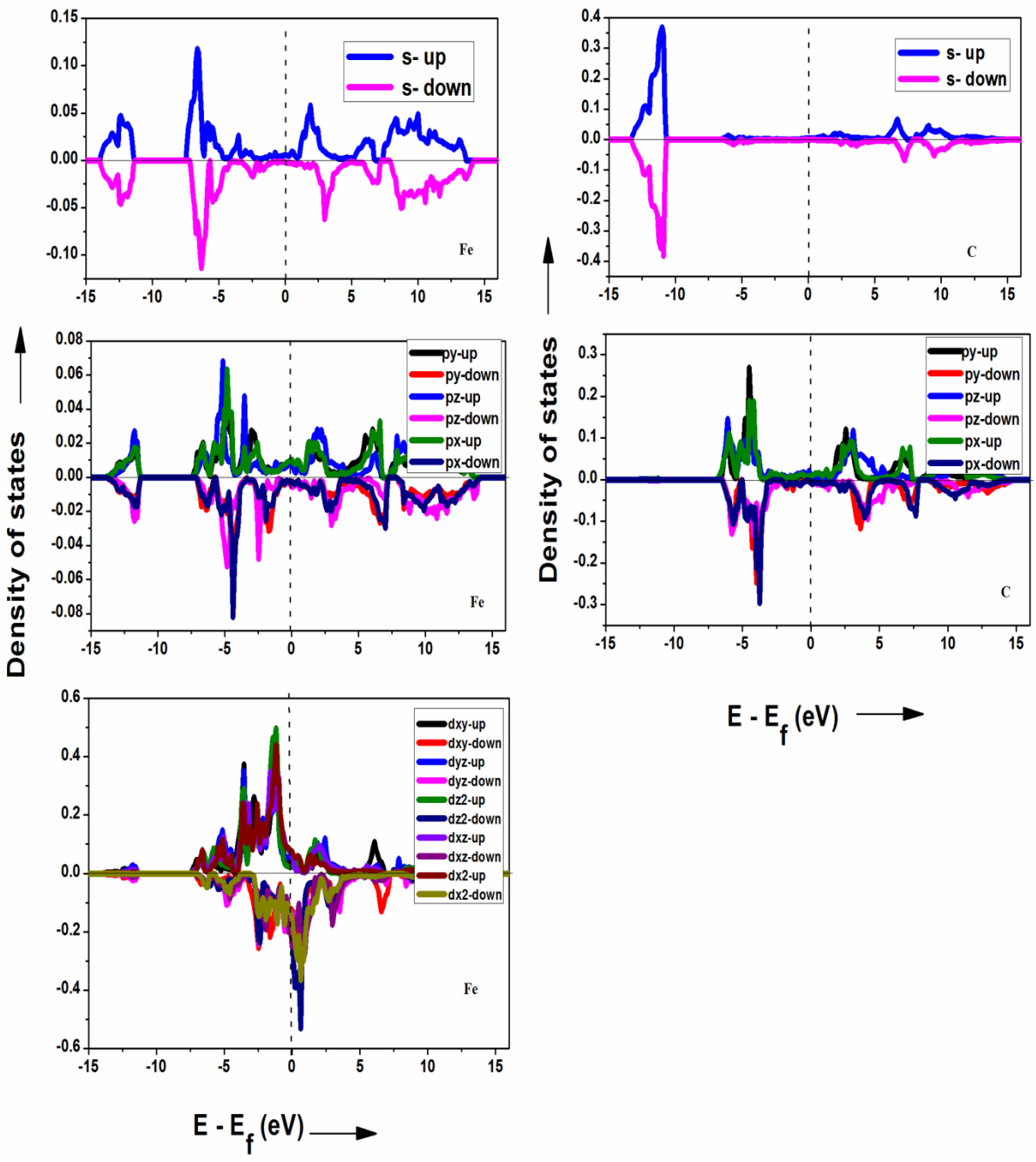

(b)

Fig 7. Partial densities of states (PDOS) of η-Fe_2C for spin-up and down states. (a) GGA-US and (b) GGA-PAW.

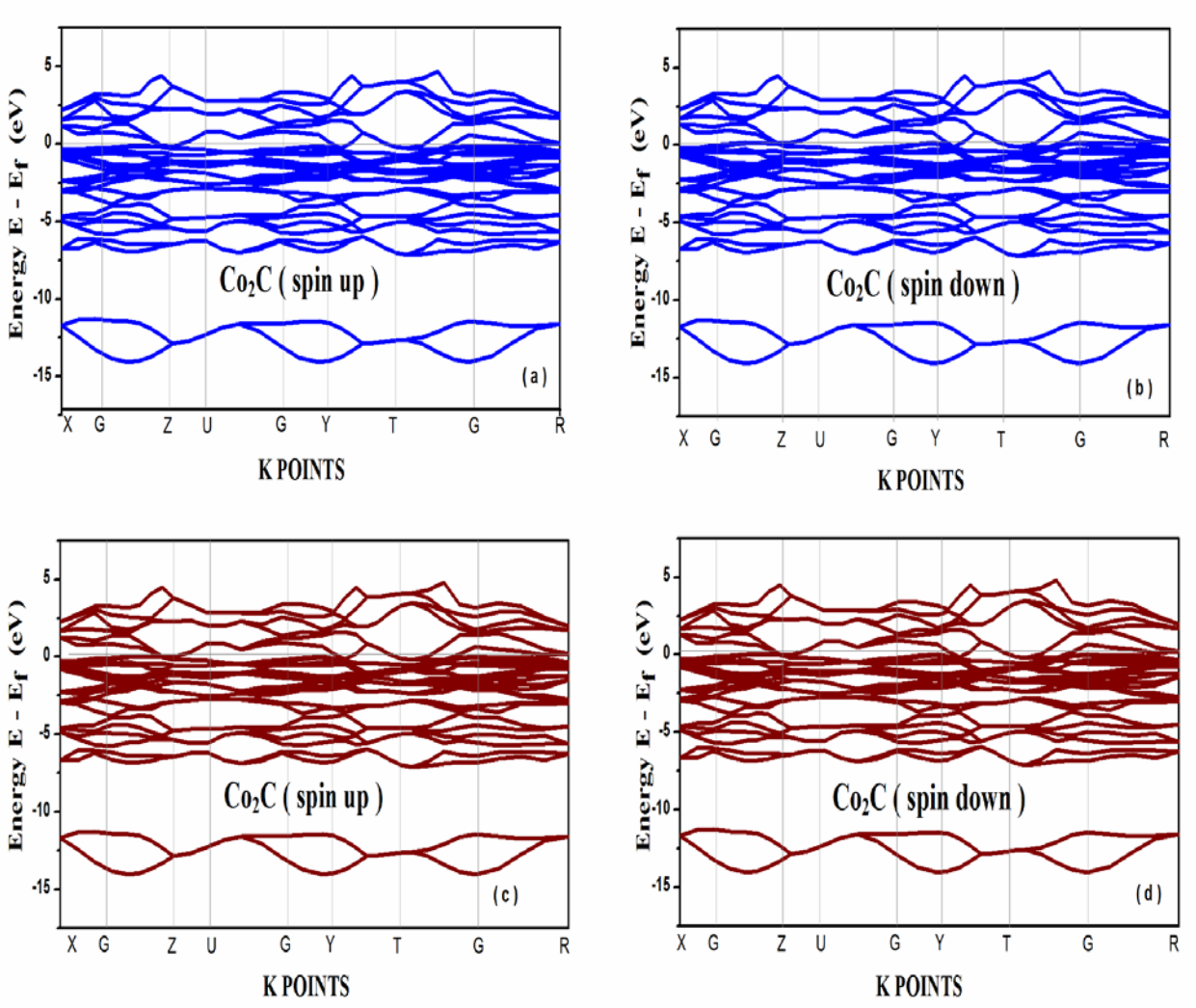

Fig 8. Electronic band structure of Co_2C. (a), (b) GGA - US and (c), (d) GGA- PAW.

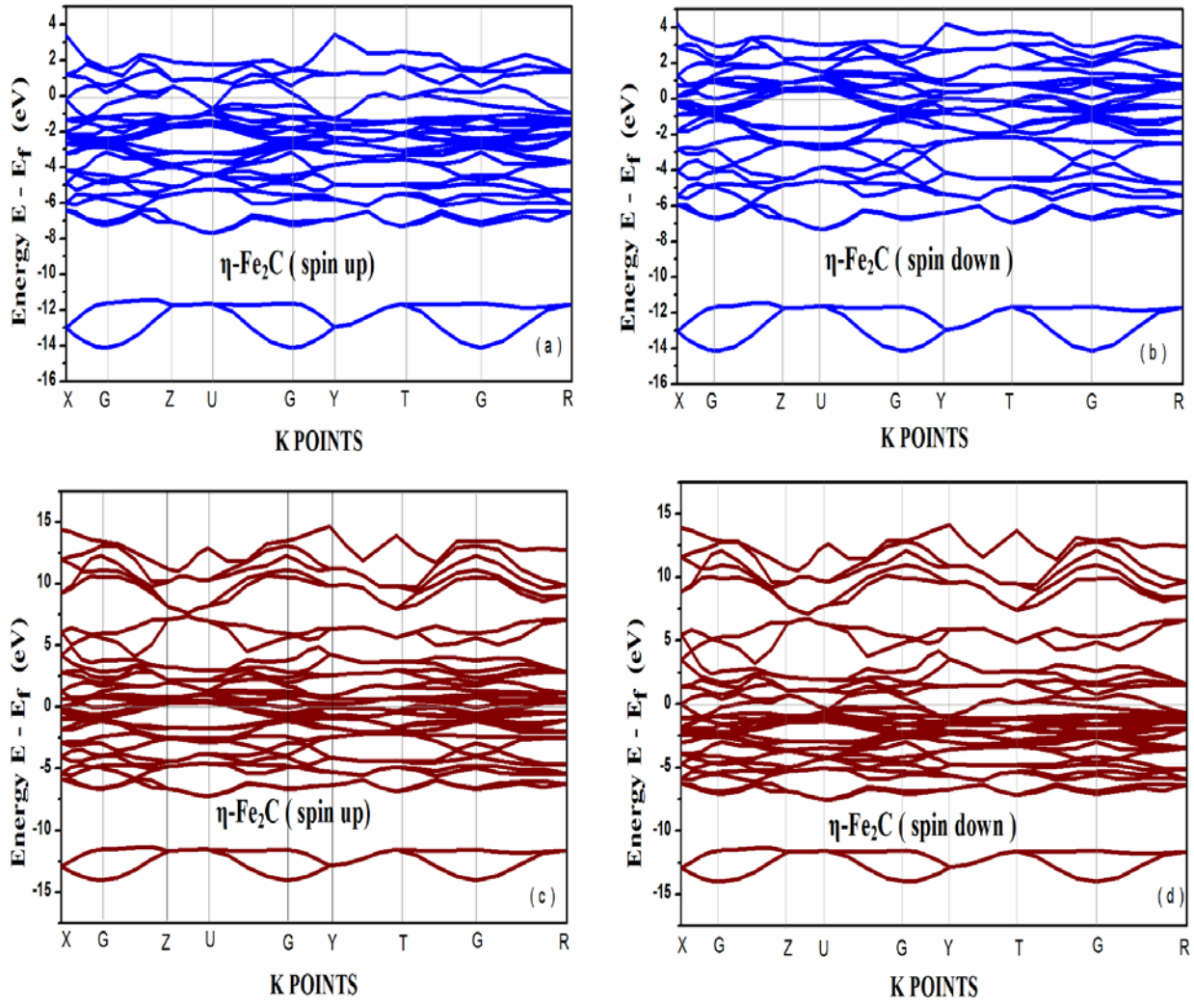

Fig 9. Electronic band structure of η- Fe_2C. (a), (b) GGA-US and (c), (d) GGA- PAW.

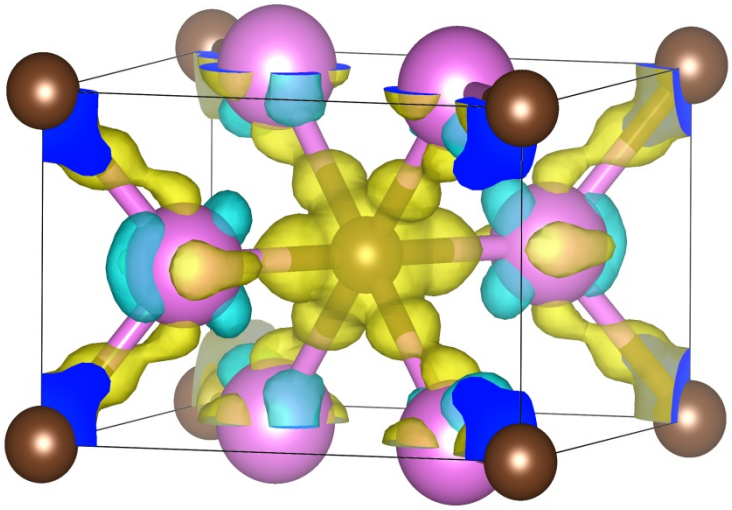

Fig 10. Valence charge density difference of Co_2C.

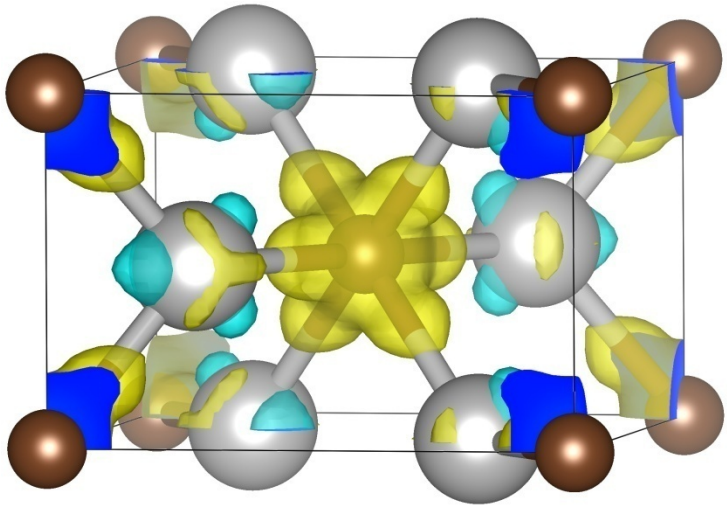

Fig 11. Valence charge density difference of η- Fe_2C.

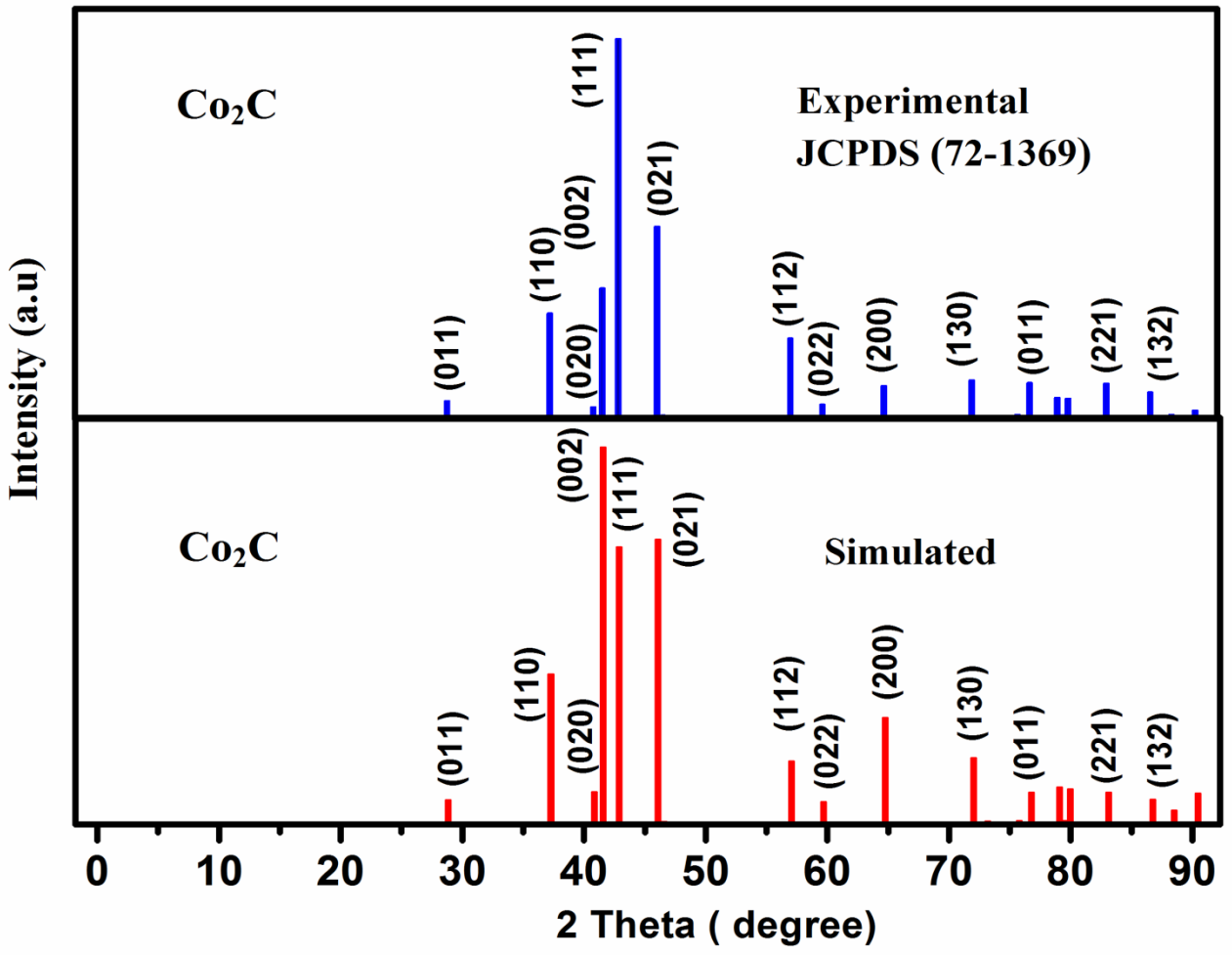

Fig 12. Comparison of experimental and simulated powder XRD patterns of Co_2C.

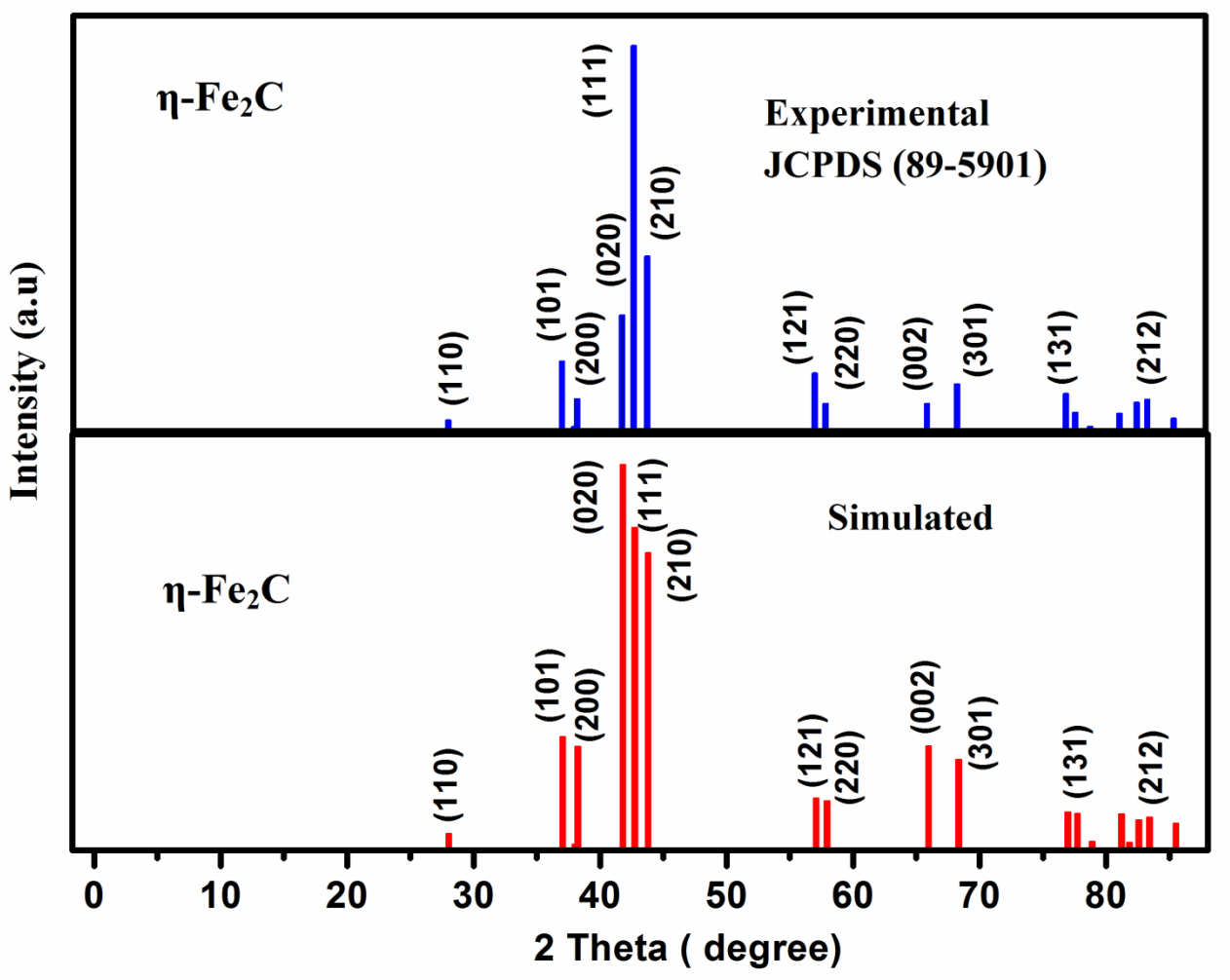

Fig 13. Comparison of experimental and simulated powder XRD patterns of η- Fe_2C.